Int. J. Heat Mass Transfer. Vol. 13, pp. 125–143. Pergamon Press 1970. Printed in Great Britain

AN EXPERIMENTAL STUDY OF THE TURBULENT PRANDTL NUMBER OF AIR WITH INJECTION AND SUCTION

R. L. SIMPSON,* D. G. WHITTEN† and R. J. MOFFAT‡

(*Received* 7 *October* 1968 *and in revised form* 27 *May* 1969)

Abstract—Experimental values for Pr_t from blown, unblown, and sucked turbulent incompressible air boundary layers ($Pr = 0{\cdot}71$) have been obtained from the mean velocity and temperature profile data of Simpson [5] and Whitten [6]. A description is given of the procedure used in obtaining these results. In the inner similarity region, $Pr_t < 1$ while $Pr_t > 1$ in the outer similarity region. These results are in agreement with Ludwieg's [2] pipe results and show no effect of blowing or suction on Pr_t.

The Jenkins model [21], which accounts for the unequal loss of momentum and thermal energy from an eddy in flight for $Pr = 1$ fluids, is found to describe the variation of Pr_t in the inner region within experimental uncertainty of the data. Using Hinze's [14] suggestion that the diffusion of heat might be a combination of gradient and large eddy transport, a new model is developed to account for $Pr_t < 1$ in the outer region. Predictions based on these models lie within the uncertainty band of the experimental results and indicate no effect of blowing or sucking on Pr_t.

NOMENCLATURE

A, $\kappa/\rho c_p$, molecular thermal diffusivity [ft²/s];
a_n, coefficients in equation (21);
B, $(\rho V)_w/(\rho U)_\infty(C_f/2)$, momentum blowing parameter;
B_{St}, $(\rho V)_w/(\rho U)_\infty(St)$, thermal blowing parameter;
$C_f/2$, friction factor;
cp, specific heat, constant pressure [Btu/lbm-°R];
d, e, constants for a given flow;
f, a function;
$G(\eta)$, a function proportional to $\frac{1}{2}V_p\overline{q^2}$;
g, h, constants for a given flow;
i, j, integers used in equation (21);
J, Pr_t from the Jenkins model, equation (26);
$K_{ij}(y)$, dependent variable in equation (21);
L, characteristic length [ft];
l, mixing length defined by equation (22) [ft];
$\dot{m}''$, $(\rho V)_w$ [lbm/s-ft²];
n, an integer;
m, p, constants for a given flow;
Pr, ν/A, molecular Prandtl number;
Pr_t, $\varepsilon_M/\varepsilon_H$, turbulent Prandtl number;
$\dot{q}''$, heat flux [Btu/s-ft²];
$\overline{q^2}$, $u^2 + v^2 + w^2$, [ft²/s²];
Re_L, $U_\infty L/\nu_\infty$, L length Reynolds number;
r, s, constants for a given flow;
St, $[\dot{q}''_w/(\rho U)_\infty c_p(T_w - T_\infty)]$, Stanton number;
T, time-averaged temperature [°R];
$\bar{T}$, $(T_w - T)/(T_w - T_\infty)$, dimensionless temperature;

* Dept. Mechanical Engineering, Southern Methodist University, Dallas, Texas 75222, U.S.A.
† Shell Development Company, Houston, Texas 77001, U.S.A.
‡ Dept. Mechanical Engineering, Stanford University, Stanford, California 94305, U.S.A.

T^+, $\overline{T}U_\tau/StU_\infty$, dimensionless temperature;
t, fluctuation temperature [°R];
U, mean velocity in the main-stream direction [ft/s];
U^+, U/U_τ, dimensionless velocity;
U_τ, $\sqrt{(\tau_w g_c/\rho)}$ [ft/s];
u, v, w, fluctuation velocities in the X, y and z-directions, respectively [ft/s];
V, mean velocity perpendicular to the surface [ft/s];
V_E, characteristic large eddy velocity [ft/s];
V_p, turbulent energy diffusion velocity [ft/s];
V_w^+, V_w/U_τ, dimensionless injection velocity [ft/s];
X, distance along the plate in the flow direction [ft];
y, perpendicular distance from the surface [ft];
y^+, yU_τ/ν, dimensionless distance;
$Z(y)$, independent variable function, equation (21);
z, distance mutually perpendicular to X and y [ft];
Δ, $\int_0^\infty (\rho U/\rho_\infty U_\infty)(1 - \overline{T})\,dy$, enthalpy thickness [ft];
Δ_r, defined by equation (16) [ft];
Δ^*, $\int_0^\infty (\rho U/\rho_\infty U_\infty)(1 - \overline{T}^2)\,dy$;
δ, boundary layer thickness, y where $U/U_\infty = 0{\cdot}99$ in. external flow; also a pipe radius [ft];
δ^*, $\int_0^\infty [1 - (\rho U/\rho_\infty U_\infty)]\,dy$, displacement thickness [ft];
ε_H, eddy thermal diffusivity [ft²/s];
ε_M, eddy kinematic viscosity [ft²/s];
ε_T, thermal gradient eddy diffusivity as in equation (27) [ft²/s];
ζ, defined by equation (18);
η, y/δ, dimensionless distance;
θ, $\int_0^\infty (\rho U/\rho_\infty U_\infty)[1 - (U/U_\infty)]\,dy$, momentum thickness [ft];
θ_r, defined by equation (15);
θ^*, $\int_0^\infty (\rho U/\rho_\infty U)[1 - (U/U_\infty)^2]\,dy$, mechanical energy thickness [ft];
κ, molecular thermal conductivity [Btu/s-ft-°R];
λ, dummy variable;
μ, viscosity [lbm/s-ft];
ν, kinematic viscosity [ft/s];
ξ, defined by equation (17);
ρ, density [lbm/ft³];
τ, shear stress [lbf/ft²].

Subscripts

f, denotes final condition;
i, indicates initial condition;
t, denotes turbulent contribution;
w, indicates wall condition;
∞, denotes free-stream condition.

1. INTRODUCTION

As is well known, there exists at the present time no purely theoretical solution of the fluid dynamics of the turbulent boundary layer. Consequently there is no theoretical solution available for heat transfer in the turbulent boundary layer. In the momentum problem the "eddy viscosity" remains unknown while the "eddy conductivity" is unspecified in the case of heat transfer.

The classical approach to obtaining the transport mechanism for the heat transfer problem follows the laminar approach; namely, the momentum and thermal transport mechanisms are related by a factor, the Prandtl number Pr. Hence, combining the laminar and "eddy" viscosities one obtains the Boussinesq relation

$$\frac{\tau g_c}{\rho} = (\nu + \varepsilon_M)\frac{\partial U}{\partial y} \tag{1}$$

for the shear stress and the analogous relation

$$\frac{\dot{q}''}{\rho c_p} = -\left(\frac{\nu}{Pr} + \frac{\varepsilon_M}{Pr_t}\right)\frac{\partial T}{\partial y} \tag{2}$$

for the heat flux. The quantity Pr_t is known as the turbulent Prandtl number.

Thus if one knows the eddy viscosity and the turbulent Prandtl number the heat transfer problem can be solved. A number of experimental and theoretical investigations have been devoted to obtaining the eddy viscosity. Only a few studies have been made of the turbulent Prandtl number. No previous experimental studies have been reported on the effect of blowing or suction on Pr_t.

1.1 *Review of previous works*

Kestin and Richardson [1] recently reviewed the status of the turbulent Prandtl number. They found that the results from the few experimental studies were in conflict. The results from mercury experiments in pipes indicated that $Pr_t > 1$ while gas experiments in pipes showed $Pr_t < 1$. Thus it is not clear whether the turbulent Prandtl number is completely independent of the molecular Prandtl number. The results of Ludwieg [2], as shown in Fig. 1, and others [1] for air flowing in a pipe do not agree.

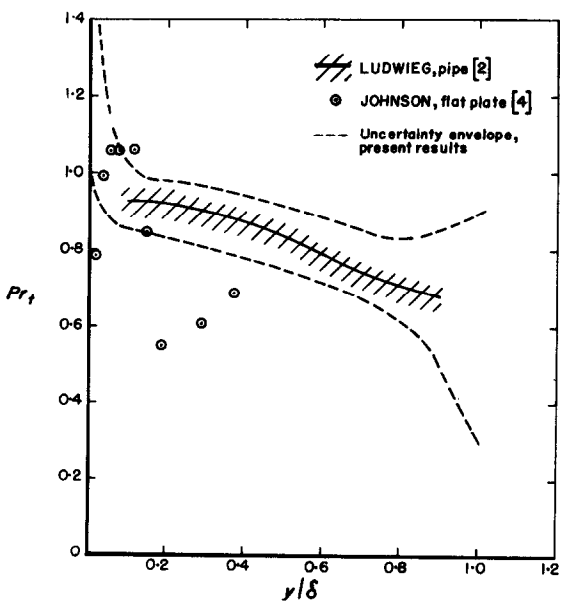

FIG. 1. Comparison of experimental results.

In a brief account of these investigations, Kestin and Richardson [1] concluded that Ludwieg's results are the most reliable for air flowing in a pipe. The flow at the center of a pipe does not include regions of intermittent wake-like flow, such as occur in the outer region of an external boundary layer. On extrapolation of Ludwieg's results on the basis of the reciprocal of distance from the wall, they found that his measured values were asymptotic to a turbulent Prandtl number of 0·5 at large distances from the wall. This is in agreement with the value of 0·5 deduced by Fage and Faulkner [3] from the wake of a cylinder and by Reichardt [1] in a free jet. The value of 0·5 is also obtained from Taylor's vorticity transport theory [3], which gives further support to the trend of Ludwieg's results.

The only experimental study of Pr_t on a flat plate with a constant free-stream velocity known to the authors was reported by Johnson [4], who used hot-wire anemometers to determine the distribution of velocity and temperature fluctuation levels. He studied the temperature distribution downstream of an unheated starting length where the thermal boundary layer was contained at all times in an inner fraction of the momentum boundary layer, providing no information about the outer region. Johnson compared the turbulent shearing stress and the heat flux obtained by hot wire measurements with those generated from mean velocity and temperature distributions, finding a 50 per cent discrepancy in the shearing stresses and good agreement for the heat fluxes. He noted that the skin-friction coefficients obtained by several independent methods did not agree. The anomalous behavior was attributed to three-dimensionality of the flow. As shown on Fig. 1, the scatter of the Pr_t data points is considerable. Even so, the average of these results near $y/\delta \approx 0{\cdot}1$ is in fair agreement with Ludwieg's results.

As concluded by Kestin and Richardson, the question of the turbulent Prandtl number is unresolved and merits further experimental investigation not only for air but for fluids of a wide range of molecular Prandtl number.

1.2 *Objectives of the present work*

There is little consistent experimental evidence as to the distribution of Pr_t in the boundary layer on a flat plate for air. There exists no published experimental study of the effect of blowing and suction on the turbulent Prandtl number.

The Pr_t can be determined by measurements of velocity and temperature distributions in the boundary layer, and the heat flux and shear stress at the wall. Such measurements have been reported by Simpson [5] and Whitten [6] for a wide range of blowing and suction conditions with constant free-stream velocity and constant wall temperature. The blowing conditions were such as to hold the blowing parameter B constant. The experimental Stanton number and skin-friction coefficient results associated with these data have been previously described [5–8]. A description has been given of the flow characteristics associated with these data [5, 7].

In broad terms, the objectives of the present work are to determine the turbulent Prandtl number Pr_t for air from the data of Simpson and Whitten and to compare these results with available theories.

2. EXPERIMENTAL APPARATUS

The Stanford Heat and Mass Transfer Apparatus, as described in detail by Moffat and Kays [9, 10], was used in these experiments. This apparatus consists of a 24-plate porous surface, 8 ft long and 18 in. wide. The plates, each containing electric heater wires, form the lower surface of a test duct of rectangular cross section, 20 in. wide and 6 in. high at the inlet end of the duct. Separate main-stream and transpiration blowers provide the system with air, while heat exchangers are used to control air temperature.

A boundary layer trip is located just upstream of the leading edge of the porous surface. The upper surface of the duct is adjustable to achieve a uniform velocity along the duct, regardless of the distribution of the blowing or suction along the porous surface. A potential flow region, uniform within $\pm 0{\cdot}4$ per cent in velocity and $\pm 0{\cdot}25°F$ in temperature, existed for the full length of the test duct for all present blowing and suction conditions [5, 7].

The $\frac{1}{4}$in. thick sintered bronze plates have been shown to be aerodynamically smooth for the present experimental conditions [5, 7]. They are uniform in porosity within 6 per cent in the 6in. span centered on the test duct centerline, where velocity and temperature profiles are taken. The flow through each plate is individually controlled. Viscous forces govern the flow through each plate surface, preventing localized jetting of fluid to or from the boundary layer.

All measurement of gas temperatures were made with iron–constantan thermocouples, calibrated within $\pm 0{\cdot}10°F$ and described in detail by Moffat and Kays [9] and Whitten [6]. Calibrated rotameters were used to measure injection and suction flow rates: local injection rates were determined from the total flow through each plate by use of a permeability distribution map of each plate.

Mean velocity and temperature profiles were measured with stagnation pressure and thermocouple probes and manual traversing equipment, described in detail by Simpson [5] and Whitten [6]. The probes were attached to traversing mechanisms fastened to a rigid support frame. These spring-loaded micrometer-driven mechanisms provided for the change and measurement of probe distance from the test wall.

The stagnation probes used for boundary layer surveys have a flattened mouth, 0·010 in. × 0·035 in., formed from 0·025 in. o.d., 0·0025 in. wall thickness tubing. Static pressures from side wall taps agreed with the free-stream static pressure sensed by a pitot-static Prandtl probe. All present data was taken using the side wall taps. The dynamic pressures were measured with inclined manometers calibrated to within $\pm 0{\cdot}002$ in. of water.

The thermocouple probe had 0·375 in. of bare wire aligned parallel to the flow. The wire diameter was 0·010 in., and the weld bead was reduced to this same diameter. To obtain time-

averaged temperature profiles, the signal for each data point was integrated over a 100 s interval using an integrating digital voltmeter.

3. EXPERIMENTAL SKIN FRICTION AND HEAT TRANSFER RESULTS AND VELOCITY AND TEMPERATURE PROFILE DATA

The experimental skin friction coefficient and constant-wall-temperature Stanton number results from this apparatus have been reported in detail elsewhere [5–10]. The range of test conditions for the experiments presented here can be summarized as follows:

U_∞, fps	42–47
T_∞, °F	64–90
T_w, °F	86–112
Re_x	$1{\cdot}3 \times 10^5$–2×10^6
$\dot{m}''/(\rho U)_\infty$	− 0·0011–0·005

The Stanton number and friction factor results for the unblown case agree within 2 per cent of the expected correlations

$$\frac{C_f}{2} = 0{\cdot}0296\, Re_x^{-0{\cdot}2} \tag{3}$$

$$St = 0{\cdot}0296\, Re_x^{-0{\cdot}2}\, Pr^{0{\cdot}4} \left(\frac{T_w}{T_\infty}\right)^{-0{\cdot}4} \tag{4}$$

for $4 \times 10^5 < Re_x < 2 \times 10^6$.

The uniform injection friction factor results agree within ± 10 per cent with the experimental results of Kendall and the Stevenson, Rotta and Kinney results from the Mickley and Davis data, with the present results having the highest values [7]. For all turbulent flows examined where $V_w(X)$ varied slowly along the surface, $C_f/2$ and St were found to be functions of local Re_θ and B and Re_Δ and B_{St}, respectively. This agrees with the hypothesis that turbulent boundary layers behave according to local conditions in the absence of severe local disturbances [11].

The velocity and temperature profile data of Simpson and Whitten used in this study were obtained on the same day under the same test conditions, although not simultaneously. Due to the air temperature control by heat exchangers, temperatures were held constant within $\frac{1}{2}$ deg F on a given day. It was concluded [5] that no corrections to the velocity profile data for wall, viscous and stagnation pressure gradient effects were justified. No turbulence corrections were applied to the stagnation pressure data in obtaining mean velocities. Whitten [6] applied a small position correction to the temperature profile data to force the traverse points below $y^+ = 7$ to satisfy the viscous sublayer equation

$$\frac{\overline{T}}{St} = \frac{\rho_\infty U_\infty}{\rho_w V_w}\left\{\exp\left[\frac{\dot{q}'' y c_p}{\kappa}\right] - 1\right\} \tag{5}$$

derived from the momentum and energy equations, neglecting X derivatives. The average value of the correction was approximately 0·001 in.

To obtain mean velocity profile points at the same y positions as his temperature data points, Whitten [6] interpolated from Simpson's stagnation pressure data obtained at the same X position. He deduced the mean velocity profiles from the Bernoulli relation, using his temperature profiles and the perfect gas relation to obtain the variation of density through the boundary layer.

The unblown mean velocity profile data exhibited U^+ vs. y^+ similarity near the wall ($y^+ < 150$) for the present Reynolds number range [5,12]. The deviation of the unblown mean velocity profiles from U^+ vs. y^+ similarity in the "wake" region or outer portion near the freestream was found to be "normal" [5,12]. The criterion for normalcy of the "wake" region was that proposed by Coles [13] as a result of examination of nearly 500 unblown profiles. Simpson [5, 12] demonstrated that the blowing and suction velocity profile data exhibit a universal U^+ vs. y^+ and V_w^+ correlation. Whitten [6] demonstrated the near universal T^+ vs. y^+ character of the temperature profiles

near the wall for a given B or B_{St}, flow shown in Fig. 2.

For the range $1000 < Re_\theta < 6000$, good U/U_∞ vs. η similarity in the outer 90 per cent of the layers was observed along the flow duct for each flow with uniform injection and suction run all velocity profiles used for this study were similar within 0·02 U/U_∞ units with the average deviation about 0·01 units. Likewise, the temperature profiles were similar within 0·01 $\overline{T}$ units. (As pointed out by Simpson [5, 12], this velocity profile similarity agrees with Coles

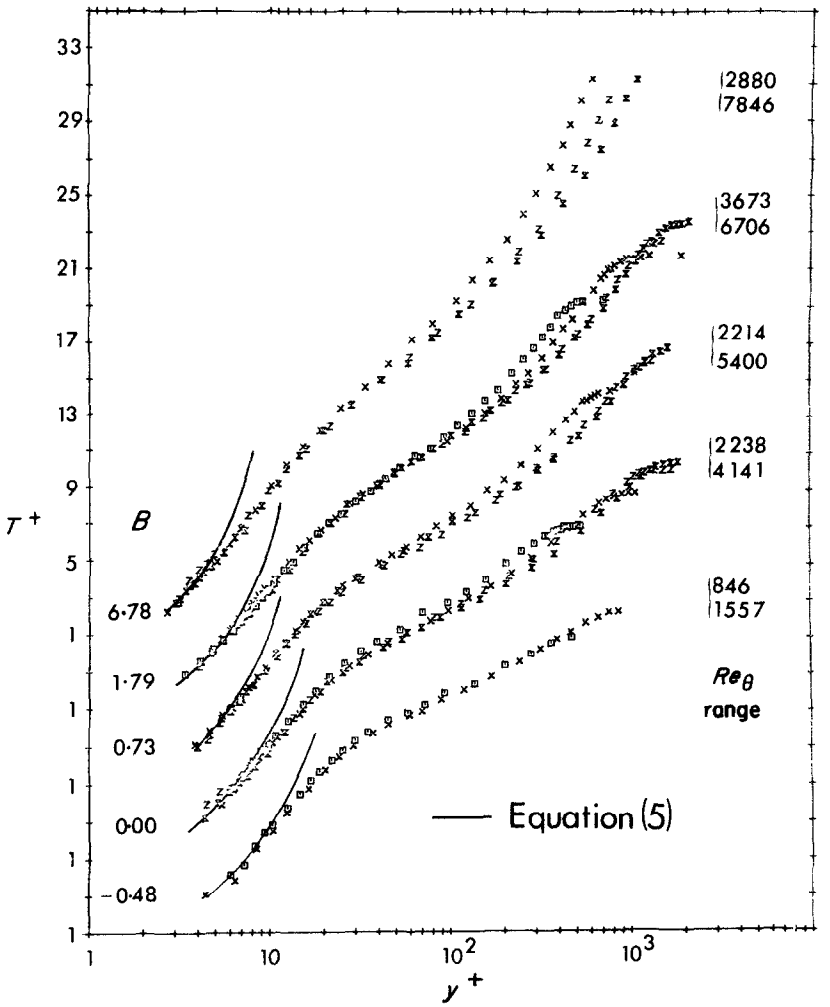

FIG. 2. Experimental temperature profiles, T^+ vs. y^+.

and with $\dot{m}'' \alpha X^{-0.2}$ [5] as shown in Fig. 3. Good $\overline{T}$ vs. η similarity was also observed for Whitten's temperature profiles with $\dot{m}'' \alpha X^{-0.2}$ [6] as shown in Fig. 4. For a given blowing or [13] conclusion that the widely accepted velocity "defect" correlation for the outer region of constant free-stream velocity unblown layers does not apply when $Re_\theta < 6000$.)

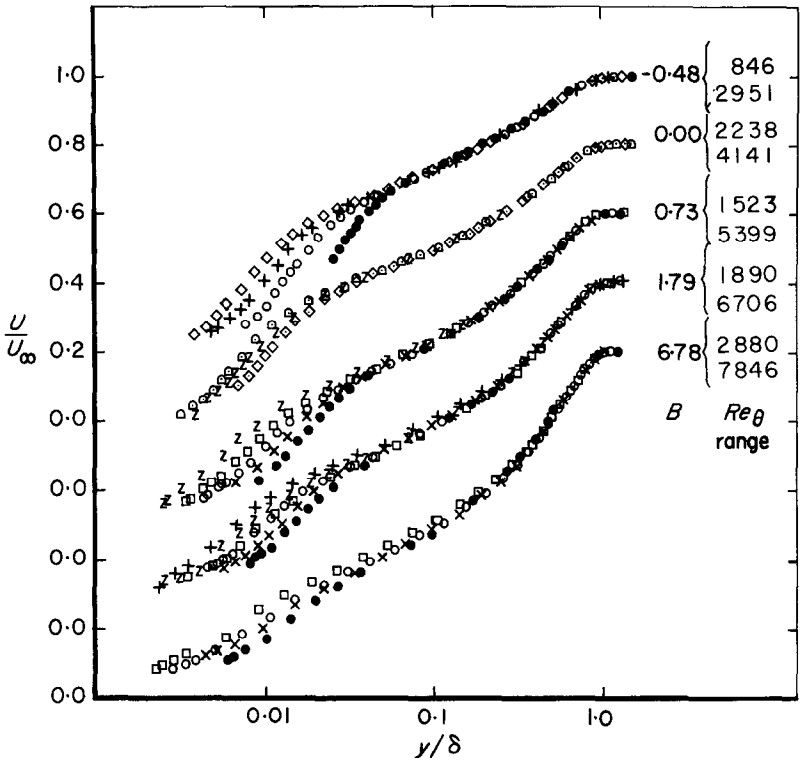

FIG. 3. Experimental velocity profiles, U/U_∞ vs. η.

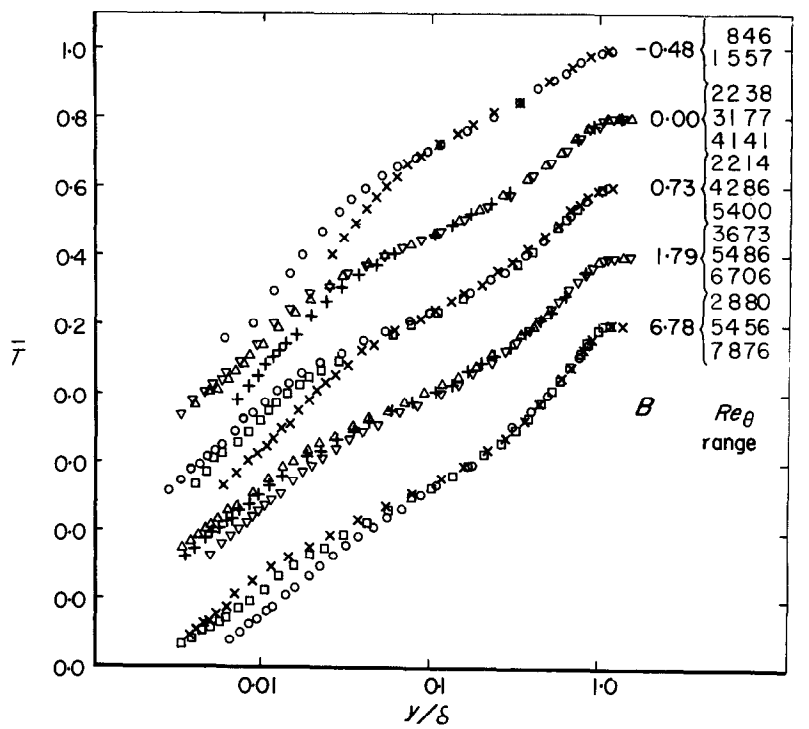

FIG. 4. Experimental temperature profiles, $\bar{T}$ vs. η.

4. SHEAR STRESS AND HEAT FLUX PROFILES

Shear stress and heat flux variations through the boundary layer must be determined to extract the turbulent Prandtl number from equations (1) and (2) using the mean velocity and temperature profile data. Mean velocity and temperature profiles were measured, and the shear stress and heat flux profiles generated from them using the time-averaged momentum, thermal energy, and continuity equations of the boundary layer.

4.1. *Boundary layer equations*

Consider the two dimensional boundary layer equations for X-momentun, thermal energy, and continuity for uniform free-stream velocity, constant wall temperature, and constant properties, with exception of the density.*

$$\frac{\partial}{\partial X}\left(\frac{\rho U^2}{\rho_\infty U_\infty^2}\right)+\frac{\partial}{\partial y}\left(\frac{\rho U V}{\rho_\infty U_\infty^2}\right)=\frac{\partial(\tau/\rho_\infty U_\infty^2)}{\partial y}\text{(momentum)} \quad (6)$$

$$\frac{\partial}{\partial X}\left(\frac{\rho U\bar{T}}{\rho_\infty U_\infty}\right)+\frac{\partial}{\partial y}\left(\frac{\rho V\bar{T}}{\rho_\infty U_\infty}\right)=\frac{\partial[\dot{q}''/\rho_\infty c_p U_\infty (T_\infty - T_w)]}{\partial y}\text{(thermal energy)} \quad (7)$$

$$\frac{\partial}{\partial X}\left(\frac{\rho U}{\rho_\infty U_\infty}\right)+\frac{\partial}{\partial y}\left(\frac{\rho V}{\rho_\infty U_\infty}\right)=0\text{ (continuity)}. \quad (8)$$

Rearranging equations (6)–(8), integrating each equation with respect to y, and applying the conditions $\rho V/\rho_\infty U_\infty = \rho_w V_w/\rho_\infty U_\infty$, $\tau = \tau_w$, and $\dot{q}'' = \dot{q}_w''$ at $y = 0$ yields

$$\frac{\partial}{\partial X}\int_0^y \frac{\rho U^2}{\rho_\infty U_\infty^2}\,dy+\left.\frac{\rho_w V_w U}{\rho_\infty U_\infty^2}\right|_0^y - \frac{U}{U_\infty}\frac{\partial}{\partial X}\int_0^y \frac{\rho U}{\rho_\infty U_\infty}\,dy=\frac{\tau-\tau_w}{\rho_\infty U_\infty^2} \quad (9)$$

$$\frac{\partial}{\partial X}\int_0^y \frac{\rho U\bar{T}}{\rho_\infty U_\infty}\,dy+\left.\frac{\rho_w V_w \bar{T}}{\rho_\infty U_\infty}\right|_0^y - \bar{T}\frac{\partial}{\partial X}\int_0^y \frac{\rho U}{\rho_\infty U_\infty}\,dy=\frac{\dot{q}''-\dot{q}_w''}{\rho_\infty U_\infty c_p(T_\infty - T_w)} \quad (10)$$

when the resulting continuity equation is substituted into the thermal energy and momentum equations.

4.2 *Computing equations*

The numerical differentiation of experimental boundary layer data with respect to X produces uncertain results when only a few X-stations are available. Therefore the following assumptions were employed to evaluate the left sides of equations (9) and (10):

1. U/U_∞ and $\bar{T}$ are each functions of y/δ only in the outer region, i.e. all X dependency is contained in δ.

2. the contributions from the convective terms containing $\partial/\partial X$, in the momentum and thermal energy equations are very small in the inner region where assumption (1) fails.

3. $(1/\theta)\,(d\theta/dx) \simeq (1/\delta)\,(d\delta/dx)$ for momentum and $(1/\Delta)\,(d\Delta/dx) \simeq (1/\delta)\,(d\delta/dx)$ for thermal energy.

Using these assumptions in equations (9) and (10) and integrating by parts yields the shear stress and heat flux computing equations for flows with small ρ/ρ_∞ variations through the boundary layer

* Implicit in the form of equations (6) and (7) is the neglect of fluctuation terms which are of higher order in flows not near boundary layer separation [11], such as those considered here.

$$\frac{\tau}{\rho_\infty U_\infty^2} = \frac{C_f}{2} + \frac{1}{\theta}\frac{d\theta}{dX}\left[\int_0^y \frac{\rho U^2}{\rho_\infty U_\infty^2}dy - \frac{U}{U_\infty}\int_0^y \frac{\rho U}{\rho_\infty U_\infty}dy\right] + \frac{\rho_w V_w U}{\rho_\infty U_\infty^2} \quad (11)$$

$$\frac{\dot{q}''}{\rho_\infty U_\infty c_p(T_\infty - T_w)} = St + \frac{1}{\Delta}\frac{d\Delta}{dX}\left[\int_0^y \frac{\rho U\bar{T}}{\rho_\infty U_\infty}dy - \bar{T}\int_0^y \frac{\rho U}{\rho_\infty U_\infty}dy\right] + \frac{\rho_w V_w \bar{T}}{\rho_\infty U_\infty}. \quad (12)$$

Equations (11) and (12) reduce to the two-dimensional momentum and thermal energy integral equations when $y \to \infty$

$$\frac{C_f}{2} = \frac{d\theta}{dX} - \frac{\rho_w V_w}{\rho_\infty U_\infty} \quad (13)$$

$$St = \frac{d\Delta}{dX} - \frac{\rho_w V_w}{\rho_\infty U_\infty}. \quad (14)$$

4.3 *Substantiating the assumptions and validating the data*

The validity of the resulting heat flux and shear stress profiles rests strongly on the validity of the assumptions. Assumption (1) rests on the similarity discussed in Section 3 and shown in Figs. 3 and 4.

Assumption (2) is concerned with the contribution from the inner region, where assumption (1) fails, to the convective quantities. Referring to equations (11) and (12) let us define:

$$\theta_r = \int_0^y \frac{\rho U^2}{\rho_\infty U_\infty^2}dy - \frac{U}{U_\infty}\int_0^y \frac{\rho U}{\rho_\infty U_\infty}dy \quad (15)$$

$$\Delta_r = \int_0^y \frac{\rho U\bar{T}}{\rho_\infty U_\infty}dy - \bar{T}\int_0^0 \frac{\rho U}{\rho_\infty U_\infty}dy \quad (16)$$

The terms on the right side of equations (15) and (16) are small near the wall and tend to cancel. In all velocity and temperature profiles used here $(\theta r/\theta)(d\theta/dx)$ and $(\Delta r/\Delta)(d\Delta/dx)$ contributed less than 2 per cent to the right sides of equations (11) and (12) at the inner edge of the U/U_∞, $\bar{T}$, and η similarity regions ($\eta < 0{\cdot}1$).

Assumption (3) is useful for several reasons. It allows equations (11) and (12) to reduce to the two-dimensional momentum and thermal energy equations as $y \to \infty$. Secondly, it allows $d\theta/dx$ and $d\Delta/dx$ to be replaced by $C_f/2 + \rho_w V_w/\rho_\infty U_\infty$ and $St + \rho_w V_w/\rho_\infty U_\infty$ to insure that τ and $\dot{q}''$ approach zero as $y \to \delta$. For all profiles used to generate Pr_t, assumption (3) was found to hold randomly within 5 per cent using $C_f/2$, St and $\rho_w V_w/\rho_\infty U_\infty$ to obtain $d\theta/dx$ and $d\Delta/dx$ and finite differences to obtain $d\delta/dx$.

As an internal check, the shear stress and heat flux profiles should certainly satisfy the integral equations

$$\frac{1}{2}\frac{d}{dRe_x}\left[Re_{\theta^*} - \int_0^{Re_x}\frac{\dot{m}''}{G}dRe_x\right] = \frac{1}{2}\frac{d\xi}{dRe_x} = \int_0^1 \frac{\tau}{\rho_\infty U_\infty^2}d\left(\frac{U}{U_\infty}\right) \quad (17)$$

$$\frac{1}{2dRe_x}\frac{d}{}\left[Re_{\Delta^*} - \int_0^{Re_x}\frac{\dot{m}''}{G}dRe_x = \frac{1}{2dRe_x}\frac{d\zeta}{}\right] = \int_0^1 \frac{\dot{q}''\,d\bar{T}}{\rho_\infty U_\infty c_p(T_\infty - T_w)} \quad (18)$$

These equations are derived by multiplying equations (6) and (7) by U/U_∞ and $\bar{T}$, respectively, integrating with respect to y, using the integral continuity equation, and letting

$y \to \infty$. Equation (17) is known as the "mean mechanical energy equation" [11].

The left sides of equations (17) and (18) can be obtained directly from data, independent of any assumptions used to generate shear stress and heat flux profiles. The right sides can be deduced from the generated shear stress and heat flux profiles. For each run a power fit of the form hRe_x^p was made of ξ and of the form $deRe_x^e$ for ζ. Differentiating the results produce $hpRe_x^{p-1}$ and $deRe_x^{e-1}$ for the left sides of equations (17) and (18). The right sides are easily fitted by mRe_x^q and rRe_x^s. As shown in reference [5], at $Re_x = 10^6$ there is a 3·5 per cent difference between the sides of equation (17) for the $B = -0{\cdot}48$ run and less than 1 per cent difference on all other flows considered here. Using $e = 0{\cdot}8$ obtained from a mass plot of all present ζ points, there is a 7 per cent difference between the sides of equation (18) for the $B = -0{\cdot}48$ run and less than 2 per cent difference on all other runs. It is concluded that the shear stress and heat flux profiles satisfy the integral momentum, continuity, thermal energy and equations (17) and (18) to a good degree.

Typical heat flux profiles for blown flows are normalized on the *maximum* heat flux and presented in Fig. 5 against $\bar{T}$ for the constant B flows discussed here. Similarly, shear stress profiles for the constant $\dot{m}''$ and constant B cases have been normalized on the maximum shear stress and presented [5,12] on plots against U/U_∞. As one can see from these plots near the wall the profiles are nearly linear and can be described by

$$\tau = \tau_w [1 + BU/U_\infty] \tag{19}$$

for the shear stress and

$$\dot{q}'' = \dot{q}''_w [1 + B_{st}\bar{T}] \tag{20}$$

for the heat flux. Equations (9) and (10) reduce to equations (19) and (20), respectively, when the convective terms are neglected. Maxima are seen to occur near $U/U_\infty = 0{\cdot}63$ for the shear stress and $\bar{T} = 0{\cdot}63$ for the heat flux. These maxima existed for all blown shear stress and heat flux profiles examined. In the outer portion ($U/U_\infty > 0{\cdot}63$, $\bar{T} > 0{\cdot}63$), all blown τ/τ_{max} vs. U/U_∞ and q''/q''_{max} vs. $\bar{T}$ profiles lie on a single curve independent of B and B_{st}.

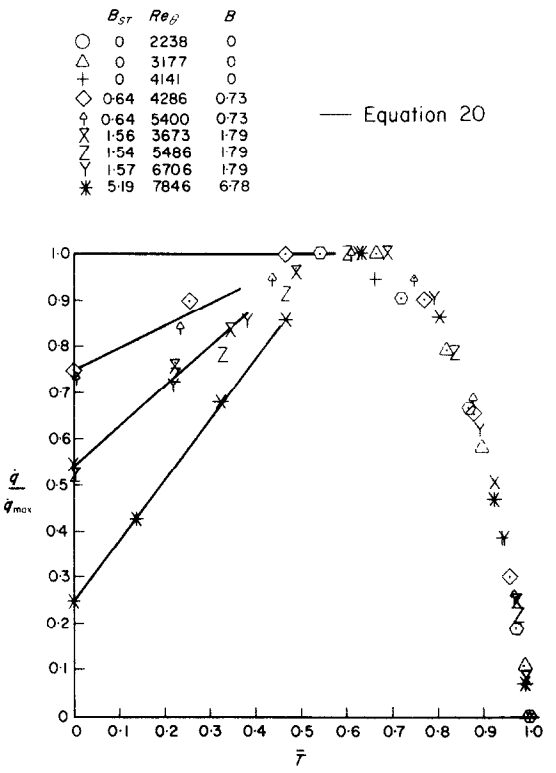

FIG. 5. Heat flux profiles, $\dot{q}''/\dot{q}''_{max}$ vs. $\bar{T}$, const. B and B_{st} flows.

5. EXPERIMENTAL RESULTS

The quantities ε_M/ν and Pr_t follow from the generated shear stress and heat flux profiles, equations (1) and (2), and the gradients $\partial U/\partial y$ and $\partial T/\partial y$. Since the numerical differentiation of experimental data can be difficult and the resulting values questionable, the following procedure was used in obtaining $\partial U/\partial y$ and $\partial T/\partial y$.

Polynomial least squares curve fits of the form

$$K_{ij}(y) = \sum_{n=0}^{n=i} a_n Z(y)^n \tag{21}$$

and of degree i were made for a given pair of U/U_∞ vs. y and $\bar{T}$ vs. y data profiles at a given X station for the j number of nearest data points surrounding and including a given point of interest. The first derivative of the equation (21) for a given point produced the derivative $\partial\bar{T}/\partial y$ or $\partial(U/U_\infty)/\partial y$ for that point. The Pr_t results from four different fits of the same velocity and temperature profiles were examined to determine the degree of bias in Pr_t produced by the choice of polynomial fit. The polynomial fits tested contained: (1) $i = 2, j = 5$, and $Z(y) = y$; (2) $i = 3, j = 5$, and $Z(y) = y$; (3) $i = 2, j = 7$, and $Z(y) = y$; and (4) $i = 2, j = 5$, and $Z(y) = \ln|y|$. For a given pair of velocity and temperature profiles, the resulting Pr_t profiles differed by no more than 2 per cent depending on the choice of polynomial fit. The results for $i = 2$, $j = 5$ and $Z(y) = \ln|y|$ are presented here.

In addition, $\partial\bar{T}/\partial y$ and $\partial(U/U_\infty)/\partial y$ were obtained graphically. The resulting Pr_t distributions were found to be within 5 per cent agreement with the $i = 2$, $j = 5$, and $Z(y) = \ln|y|$ polynomial fit results for the same set of profiles.

It is well known [11, 14] that near the wall the flow is governed by the wall condition, molecular viscosity, and small scale turbulence. For a given blowing condition or V_w^+, U^+ and ε_M/ν correlate with y^+, indicating the importance of ν in production of the small scale turbulence and supporting the validity of equation (1) near the wall [12]. In the outer region eddy motion determines the momentum transport with the mean velocity profile and dimensionless eddy viscosity $\varepsilon_M/\delta^* U_\infty$ profile correlating on η and slightly on Re_θ for a given blowing condition [12]. Thus ν plays a rather small role in this region, being contained explicitly only in Re_θ.

The present values for the unblown ε_M/ν profiles near the wall were compared [12] with ε_M/ν results from hot-wire anemometer data using the results of Kline [15] from the data of Klebanoff [16] and the results of Hinze [14] from the data of Schubauer [17]. For a given y^+ the present results agreed within 5 per cent and within the scatter of the Kline and Hinze results for the region of U^+ vs. y^+ similarity and $y^+ > 20$ ($\varepsilon_M/\nu > 4$). In the outer region the generated $\varepsilon_M/\delta^* U_\infty$ vs. η profile was within 7 per cent agreement of the Bradshaw [18] profile from the Klebanoff data [16] for approximately the same Re_θ [12]. This good agreement with previously obtained eddy viscosity results supports the general acceptability of the present method in obtaining ε_M/ν not extremely close to the wall ($\varepsilon_M/\nu > 4$).

The molecular property ν plays a strong role in the transport of momentum near the wall, and the molecular property A or ν/Pr is important in the transport of heat in this region. This suggests that Pr_t might be correlated against a quantity containing ν or A. Hence, the experimental Pr_t results from all blown and sucked velocity and temperature profiles used here are plotted in Fig. 6 vs. y^+ and in Fig. 7 vs. ε_M/ν.

Although y^+ is the characteristic dimensionless length for the inner region only, Pr_t is still well correlated by y^+ in the outer region $y^+ > 150$) where $Pr_t < 1{\cdot}0$. In Fig. 7 Pr_t appears to be double-valued for a given ε_M/ν. This is due to the fact that ε_M/ν increases from the wall to some maximum value and then decays toward zero as $\eta \to 1$ while Pr_t decreases monotonically from the wall. Note that ε_M/ν fails to correlate Pr_t for the outer flow region, where Pr_t is less than one. Since η appears to be the characteristic coordinate for correlating results in the outer region, the Pr_t results are presented in that form in Fig. 8.

Surrounding the mean value lines on Figs. 6–8 are uncertainty envelopes for 20:1 odds calculated by the method of Kline and McClintock [19] using estimated uncertainties given in references [5] and [6] for St, $C_f/2$, U/U_∞, $\bar{T}$ and y. With exception of several data points, well within the 20:1 odds, the results fall within these uncertainty envelopes. Shown in Figs. 6 and 7 are large uncertainties near $y^+ = 10$ and $\varepsilon_M/\nu = 1$, due partly to uncertainties in locating the probes relative to the wall and

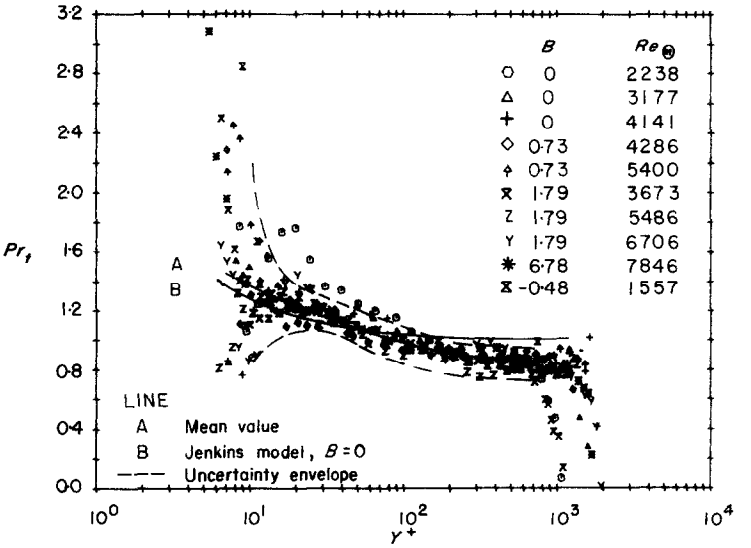

FIG. 6. Experimental results, Pr_t vs. y^+.

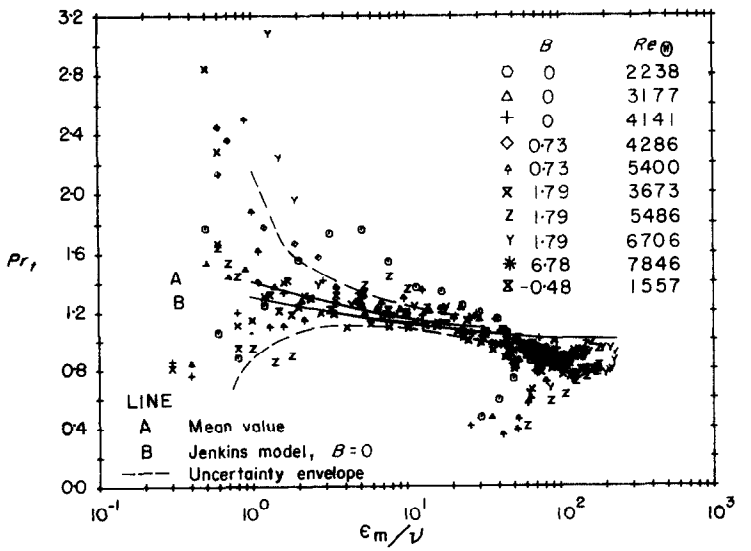

FIG. 7. Experimental results, Pr_t vs. ε_M/ν.

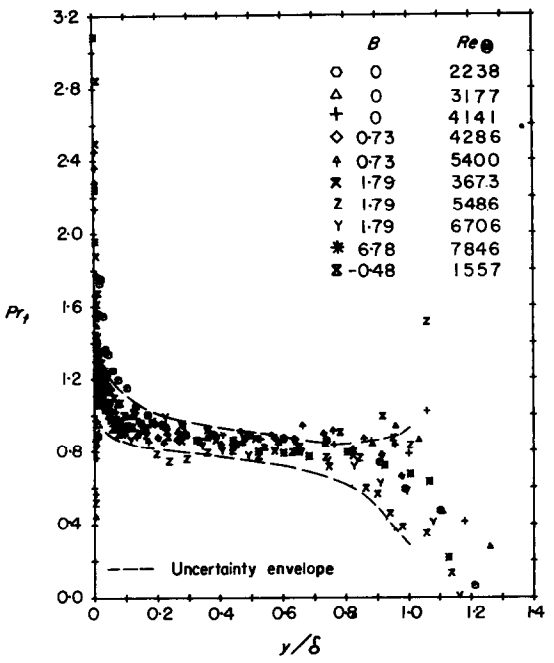

FIG. 8. Experimental results, Pr_t vs. η.

partly to the small turbulent transport relative to the total contribution. The large uncertainty near $\eta = 1$, as shown in Fig. 8, is due to τ, $\dot{q}''$, $\partial U/\partial y$ and $\partial \overline{T}/\partial y$ all approaching zero.

In the intermediate range, $\varepsilon_M/\nu > 4$, $y^+ > 20$, and $y/\delta < 0{\cdot}8$, the uncertainties mask any effects of blowing or sucking on Pr_t. In Fig. 6 no distinct effect of blowing or sucking can be determined when Pr_t is plotted against y^+. Even using $\varepsilon_M/\nu = f(V_w^+, y^+)$ [12], no effect of V_w^+ is seen in Fig. 7 because the variation of ε_M/ν with V_w^+ is contained within the uncertainty envelope. Likewise in Fig. 8, no discernable effect of blowing or sucking can be seen.

On Fig. 1 all present results are compared with Ludwieg's pipe results and Johnson's flat plate results. Ludwieg's results and the present results overlap, indicating agreement within the experimental uncertainties. One may, at first be surprised that these results agree for $y/\delta \geqslant 0{\cdot}1$, since the flow at the center of a pipe does not include the intermittent wake-like flow that occurs in the outer region of a flat plate layer. However, Townsend [20] noted that the turbulence structure away from the wall in these two types of flow partly consists of large scale eddies of the order of δ or the pipe radius in size. Thus, it appears that the large eddy structure influences the transport of heat and momentum in both pipe and external flows.

6. THEORETICAL CONSIDERATIONS*

Reynolds [1] was the first to assume that $Pr_t = 1$ on the basis of a heuristic argument which notes that in a fully turbulent field, both momentum and heat are transferred as a result of eddies. From Figs. 6–8 one can see that Reynolds' argument fails to hold in detail throughout the boundary layer. The local value of $Pr_t > 1$ near the wall ($y^+ < 150$) where the small scale turbulence is strongly affected by molecular kinematic viscosity. The $Pr_t < 1$ in the outer region ($\eta > 0{\cdot}05$) where ν has little influence. Likewise, it is suspected that A affects the transport of heat near the wall and has little influence in the outer region.

6.1 *Inner region, $Pr_t \geqslant 1$: background information*

Jenkins [21] devised a model to account for the unequal loss of momentum and thermal energy from an eddy in flight between mixing points for a $Pr \neq 1$ fluid. For coherence the main points of this model are presented. He argued that if the temperature of the eddy did not change in flight, then the definition of the mixing length

$$l = \frac{\sqrt{(\tau_t/\rho)}}{\partial U/\partial y} \tag{22}$$

plus

$$\varepsilon_H \frac{\partial T}{\partial y} = \overline{tv} \tag{23}$$

* The experimental results discussed in the previous sections were deduced independently of any theory presented here.

would produce

$$\varepsilon_H = l|v| \tag{24}$$

since $|t| = l\partial T/\partial y$. However, if heat were lost during transit, then the fluctuation temperature t would actually be less than this amount because of molecular thermal conductivity, i.e.

$$\varepsilon_H = l|v|\frac{(T_f - T_i)}{l\partial T/\partial y} \tag{25}$$

where T_i and T_f are the initial and final eddy mean temperatures. Jenkins assumed that the eddies were spheres of radius l, the mixing length, with the surface temperature of the particles varying linearly with time during their movement. The time between an eddy's creation and destruction was taken as $l/|v|$. Using Carslaw and Jaeger's formula for the average temperature of a sphere under these conditions, he obtained an expression for equation (25).

Treating the effects of molecular viscosity on an eddy in flight in the same manner as the effects of molecular thermal conductivity, he obtained the following relation

$$J = \frac{1}{Pr}\left[\frac{\frac{2}{15} - \frac{12}{\pi^6}\left(\frac{\varepsilon_M}{\nu}\right)\left[\sum_{n=1}^{\infty}\frac{1}{n^6}\left(1 - \exp\frac{-n^2\pi^2}{\varepsilon_M/\nu}\right)\right]}{\frac{2}{15} - \frac{12}{\pi^6}\left(Pr\frac{\varepsilon_M}{\nu}\right)\left[\sum_{n=1}^{\infty}\frac{1}{n^6}\left(1 - \exp\frac{-n^2\pi^2}{Pr\varepsilon_M/\nu}\right)\right]}\right] \tag{26}$$

where $J = Pr_t$. The results from this equation are shown in Figs. 6 and 7 for $Pr = 0{\cdot}71$, using the unblown ε_M/ν vs. y^+ results of Hinze [14] in Fig. 6. For $\varepsilon_M/\nu < 70$ and $y^+ < 150$ the Jenkins model falls within the uncertainty of the experimental results. In the outer region $J \to 1$ and the Jenkins model clearly fails to agree with the experimental results. Although no blowing or sucking effects are explicitly included in this model, no modification to account for this seems necessary in view of the experimental results.

It is not entirely surprising that the Jenkins model agrees, within experimental uncertainty, with experiment near the wall and fails in the outer region. This model agrees with the idea that small scale wall turbulence is governed by molecular properties (near wall) but fails to account for the large eddy motion in the outer region. The following hypothesis accounts for the effect of this large eddy structure.

6.2 *An hypothesis regarding the outer region, $Pr_t \leqslant 1$**

As pointed out by Hinze [14] from the work of Townsend [20], the transfer of mainstream momentum, a vector quantity, appears to be a velocity gradient related process associated with small scale turbulence. On the other hand, turbulence energy, a scalar quantity, appears to be mostly diffused by the large eddies [18, 20], at least in the outer part of the boundary layer where the diffusion term in the turbulence energy equation is most important. This part of the turbulence energy diffusion has been represented [14, 18] by $\frac{1}{2}\rho\overline{q^2}\overline{V_p}$, where V_p is the effective velocity at which the turbulence energy $\frac{1}{2}\rho\overline{q^2}$ is transported in the y-direction by the large eddies [22]. Hinze [14] has suggested that the diffusion of heat (and other, scalars, i.e. species) might be a combination of gradient and large eddy transport of the form

$$\frac{\dot{q}_t''}{\rho c_p(T_w - T_\infty)} = \varepsilon_T\frac{\partial\overline{T}}{\partial y} + \frac{\overline{V_E t}}{(T_w - T_\infty)} \tag{27}$$

where V_E is some characteristic velocity of the large eddy motion. *The hypothesis here is that*

* The following development is offered as a possible framework for explaining the behavior of the outer region of the boundary layer (R.L.S.).

in the outer region $\varepsilon_M = \varepsilon_T$ and $|V_E| = V_p$, i.e. the Reynolds hypothesis holds for the gradient transport while the absolute value of the characteristic large eddy velocity is the same as the turbulence energy diffusion velocity.

To determine the value and variation of the quantity $\overline{V_E t}$ through a boundary layer, the following approximate model is proposed. Bradshaw [18] has noted that at the outer edge of a self-similar boundary layer flow, such as the flow considered here, V_p is equal to the mean rate of propagation of turbulent fluid into the freestream—the "entrainment velocity". Therefore for the constant free-stream velocity flows considered here

$$\frac{V_{p\infty}}{U_\infty} = \frac{\mathrm{d}(\delta - \delta^*)}{\mathrm{d}X}, \tag{28}$$

which can be obtained from mean velocity measurements. Bradshaw *et al.* [22] present an approximate function $G(\eta)$—Fig. 2a of reference [22]—proportional to the variation of $\frac{1}{2}\rho\overline{q^2}V_p/\tau$ through a boundary layer. Bradshaw [18] also showed that for a constant free-stream velocity unblown boundary layer, $\tau/\rho\overline{q^2}$ is approximately constant for $0{\cdot}2 < \eta < 0{\cdot}9$ and decreases toward zero for $\eta < 0{\cdot}2$ and $\eta > 0{\cdot}9$. Hence one obtains

$$\frac{V_p}{U_\infty} \alpha G(\eta) \frac{\tau}{\rho\overline{q^2}}. \tag{29}$$

Although no information is available for the effect of blowing or suction on $G(\eta)$ and $\tau/\rho\overline{q^2}$, it is assumed that this resulting V_p/U_∞ variation, which is roughly linear in η, applies for all cases considered here. Since V_p/U_∞ at $\eta = 1$ is approximately $V_{p\infty}/U_\infty$ and $V_p/U_\infty = 0$ at the wall

$$\frac{V_p}{U_\infty} \sim \frac{V_{p\infty}}{U_\infty}\eta. \tag{30}$$

It is assumed that $|t|$, the mixing length l, and the mean temperature gradient $\partial T/\partial y$ are related by

$$|t| \simeq l\partial T/\partial y. \tag{31}$$

Hence

$$\overline{V_E t} \simeq V_{p\infty}\eta l\frac{\partial T}{\partial y} \tag{32}$$

and equation (27) becomes

$$\frac{\dot{q}_t''}{\rho c_p U_\infty(T_w - T_\infty)} = (\varepsilon_M + V_{p\infty}\eta l)\frac{\partial \overline{T}}{\partial y}. \tag{33}$$

Thus

$$\varepsilon_H = \varepsilon_M + V_{p\infty}\eta l \tag{34}$$

and

$$Pr_t = \frac{\varepsilon_M}{\varepsilon_M + V_{p\infty}\eta l} \tag{35}$$

in the outer region $(0{\cdot}1 < \eta < 1{\cdot}0)$.

To calculate the Pr_t distribution from equation (35) for the profiles presented here, $V_{p\infty}$ was evaluated from equation (28) using the approximations

$$\frac{1}{\delta}\frac{\mathrm{d}\delta}{\mathrm{d}x} \simeq \frac{1}{\theta}\frac{\mathrm{d}\theta}{\mathrm{d}x} \text{ and } \frac{1}{\delta^*}\frac{\mathrm{d}\delta^*}{\mathrm{d}x} \simeq \frac{1}{\theta}\frac{\mathrm{d}\theta}{\mathrm{d}x}$$

as discussed in Section 4 and in reference [5]. Hence,

$$V_{p\infty} \simeq U_\infty\left(\frac{\delta - \delta^*}{\theta}\right)\left(\frac{C_f}{2} + \frac{\rho_w V_w}{\rho_\infty U_\infty}\right), \tag{36}$$

using the momentum integral equation (13) for $\mathrm{d}\theta/\mathrm{d}x$. Using experimentally obtained values [5, 12] for all quantities contained on the right sides of equations (35) and (36), the calculated results from all profiles discussed here are shown by the symbols on Fig. 9. Note that these calculated results fall within the uncertainty envelope for the experimental results presented in Fig. 8. There is no apparent effect of blowing or suction on these calculated results.

Hence, in the outer region the physical hypothesis of large eddy transport of heat but not momentum is seen to account for $Pr_t < 1$ and to adequately describe the variation of Pr_t

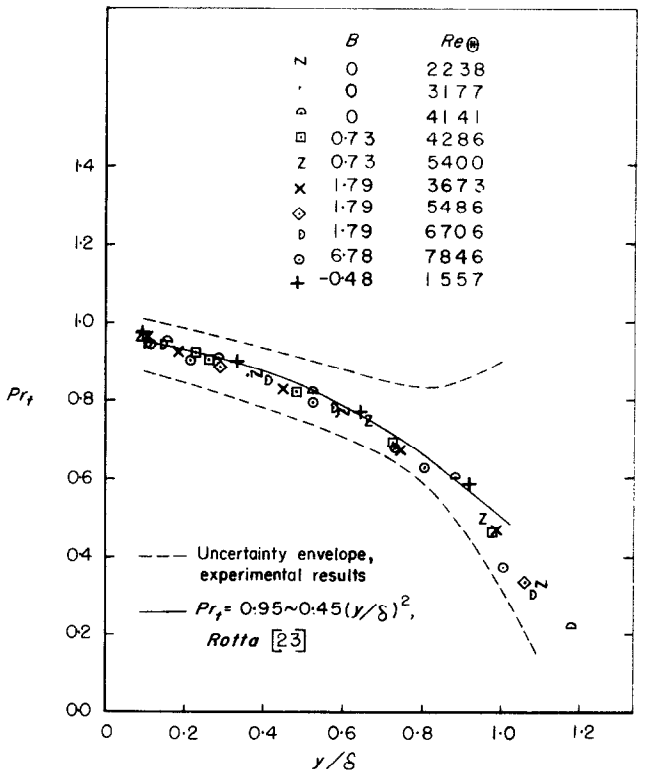

FIG. 9. Theoretical results, outer region; symbols represent results from equations (35) and (36).

within the uncertainty of the present experimental results.

6.3 *Computational relations*

One is now in a position to calculate Pr_t and hence ε_H from the turbulent flow structure of the boundary layer and the molecular Pr. In the inner region Pr_t is found to be described within experimental uncertainty, by equation (26) while equation (35) describes the outer region. For computational purposes a single relation describing both the inner and outer regions can be given by the product of equations (26) and (35)

$$Pr_t = \frac{J\varepsilon_M}{\varepsilon_M + V_{p\infty}\eta l} \tag{37}$$

Near the wall $V_{p\infty}\eta l \to 0$ and equation (37) approaches the Jenkins model. For $\eta > 0{\cdot}1$, $J \simeq 1$ and equation (37) approaches equation (35). Also shown on Fig. 9 is a purely empirical Pr_t distribution for the outer region, of the form

$$Pr_t = 0{\cdot}95 - 0{\cdot}45\,\eta^2 \tag{38}$$

as suggested by Rotta [12] for unblown flows. Using equation (38), the velocity "law of the wall" for the inner region, and the "velocity defect law" for the outer region, he calculated the Reynolds analogy factor $St/(C_f/2) = 1{\cdot}16$ for $Pr = 0{\cdot}72$. Whitten [6] obtained $St/(C_f/2) = 1{\cdot}16$ from the experimental heat transfer and skin friction results associated with the present profiles. Equation (38) is seen to agree with the calculated results within 0·05, to be within the uncertainty envelope of the experimental results, and to produce a Reynolds analogy factor

agreeing with the experimental value. Hence equation (38) should be a reliable Pr_t distribution for $0{\cdot}1 < \eta < 1{\cdot}0$ for all blown, sucked and unblown constant freestream velocity flows.

CONCLUSIONS

1. Experimental turbulent Prandtl number results from the velocity profiles of Simpson [5] and temperature profiles of Whitten [6] have been presented for constant free-stream velocity constant B flows ($-0{\cdot}48 < B < 6{\cdot}78$). A description has been given of the procedure used in obtaining these results.

2. Near the wall in the region of U^+ vs. y^+ similarity, the molecular viscosity and Prandtl number and the small scale turbulence govern the momentum and heat transport. $Pr_t > 1$ and correlates best with the inner variables ε_M/ν and y^+. In the outer region $Pr_t < 1$ and is correlated against the characteristic coordinate η. No effect of blowing or suction on Pr_t can be seen from the present experimental results.

3. The present turbulent Prandtl number results for external boundary layers agree within the experimental uncertainties with Ludwieg's pipe results [2], which were obtained for $0{\cdot}1 < \eta < 0{\cdot}9$.

4. In the inner region the Jenkins model [21] is found to describe, within experimental uncertainty, the variation of Pr_t with ε_M/ν. In the outer region, a new model for Pr_t and ε_H is developed from Hinze's [14] suggestion that the diffusion of heat might be a combination of gradient and large eddy transport. The results from both models fall within the uncertainty envelope of the experimental results and indicate no dependence of Pr_t on blowing or sucking. A composite relation describing Pr_t in both the inner and outer regions can be formed from these two models.

ACKNOWLEDGEMENTS

The authors are indebted to Messrs David W. Kearney and Robert J. Loyd of Stanford University for programming the computer to obtain the results from the experimental velocity and temperature profiles.

REFERENCES

1. J. KESTIN and P. D. RICHARDSON, Heat transfer across turbulent, incompressible boundary layers, *Int. J. Heat Mass Transfer* **6**, 147–189 (1963).
2. H. LUDWIEG, Bestimung des Verhaltnisses der Austauschkoeffizienten fur Warme and Impuls bei turbulenten Grenzschichten, *Z. Flugwiss* **4**, 73–81 (1956).
3. H. SCHLICHTING, *Boundary Layer Theory*. McGraw-Hill, New York (1960).
4. D. S. JOHNSON, Velocity and temperature fluctuation measurements in a turbulent boundary layer downstream of a stepwise discontinuity in wall temperature, *J. Appl. Mech.* **26**, 325–336 (1959).
5. R. L. SIMPSON, The turbulent boundary layer on a porous plate: an experimental study of the fluid dynamics with injection and suction, Ph.D. Thesis, Thermosciences Division, Mech. Engng Dept. Stanford Univ. (1967); available from Univ. Microfilms, Ann Arbor, Mich.
6. D. G. WHITTEN, The turbulent boundary layer on a porous plate: experimental heat transfer with variable suction, blowing, and surface temperature, Ph.D. Thesis, Thermosciences Division, Mech. Engng Dept., Stanford Univ. (1967); available from Univ. Microfilms, Ann Arbor, Mich.
7. R. L. SIMPSON, R. J. MOFFAT and W. M. KAYS, The turbulent boundary layer on a porous plate: experimental skin friction with variable injection and suction. *Int. J. Heat Mass Transfer* **12**,, 771–791 (1969).
8. D. G. WHITTEN, W. M. KAYS and R. J. MOFFAT, The turbulent boundary layer on a porous plate: experimental heat transfer with variable suction, blowing, and surface temperature, *Int. J. Heat Mass Transfer* (to be published).
9. R. J. MOFFAT and W. M. KAYS, The turbulent boundary layer on a porous plate: experimental heat transfer with uniform blowing and suction, Report HMT-1, Thermosciences Division, Dept. of Mech. Engrg., Standford Univ. (1967).
10. R. J. MOFFAT and W. M. KAYS, The turbulent boundary layer on a porous plate: experimental heat transfer with uniform blowing and suction, *Int. J. Heat Mass Transfer* **11**, 1947–1965 (1968).
11. J. C. ROTTA, Turbulent boundary layers in incompressible flow, *Progress in Aeronautical Sciences*, edited by A. FERRI, D. KUCHEMANN and L. STERNE Vol. 2, pp. 1–219. Macmillan, New York (1962).
12. R. L. SIMPSON, Characteristics of turbulent boundary layers at low Reynolds numbers with and without transpiration, *J. Fluid Mech.*
13. D. E. COLES, The turbulent boundary layer in a compressible fluid, RAND Report R-403-PR (1962).
14. J. O. HINZE, *Turbulence*. McGraw-Hill, New York (1959).
15. S. J. KLINE, Some remarks on turbulent shear flows, *Proc. Inst Mech. Engrs* **180**, part 3J, 222–224 (1965).
16. P. S. KLEBANOFF, Characteristics of turbulence in a boundary layer with zero pressure gradient, NACA TN 3178 (1954).

17. G. B. SCHUBAUER, Turbulent processes as observed in boundary layer and pipe, *J. Appl. Phys.* **25**, 188–196 (1954)
18. P. BRADSHAW, The turbulence structure of equilibrium boundary layers, *J. Fluid Mech.* **29**, part 4, 625–645 (1967).
19. S. J. KLINE and F. A. MCCLINTOCK, Describing uncertainties in single sample experiments, *Mech. Engrs* **75**, 3–8 (1953).
20. A. A. TOWNSEND, *The Structure of Turbulent Shear Flow* University Press, Cambridge (1956).
21. R. JENKINS, Variation of the eddy conductivity with Prandtl modulus and its use in prediction of turbulent heat transfer coefficients, *Inst. Heat Transfer Fluid Mech.* 147–158 (1951).
22. P. BRADSHAW, D. H. FERRISS and N. P. ATWELL, Calculation of boundary-layer development using the turbulent energy equation, *J. Fluid Mech.* **28**, part 3, 593–616 (1967).
23. J. C. ROTTA, Temperaturverteilungen in der Turbulenten Grenzschicht an der Ebenen Platte, *Int. J. Heat Mass Transfer* **7**, 215–228 (1964).

ETUDE EXPÉRIMENTALE DU NOMBRE DE PRANDTL TURBULENT DE L'AIR AVEC INJECTION ET ASPIRATION

Résumé—Les valeurs expérimentales pour Pr_t des couches limites turbulentes incompressibles d'air ($Pr = 0{,}71$) soufflées, aspirées ouvnon, ont été obtenues à partir des résultats des profils de vitesse et de température moyennes de Simpson [5] et Whitten [6]. Le procédé employé pour obtenir ces résultats est décrit. Dans la région de similitude intérieure, $Pr_t > 1$ tandis que $Pr_t < 1$ dans la région de similitude extérieure. Ces résultats sont en accord avec ceux de Ludwieg [2] pour un tuyau et ne montrent aucun effet du soufflage ou de l'aspiration sur Pr_t.

Le modèle de Jenkins [21], qui tient compte de l'inégalité entre la perte de quantité de mouvement et celle de l'énergie thermique à partir d'un tourbillon en mouvement pour des fluides avec $Pr = 1$, décrit la variation de Pr_t dans la région intérieure en tenant compte de l'incertitude expérimentale des données. En employant la suggestion de Hinze [14] que la diffusion de la chaleur pourrait être une combinaison d'un transport par gradient et par de grands tourbillons, un nouveau modèle est élaboré pour tenir compte de ce que $Pr_t < 1$ dans la région extérieure. Les prévisions basées sur ces modèles se trouvent dans la bande d'incertitude des résultats expérimentaux et n'indiquent aucun effet du soufflage ou de l'aspiration sur Pr_t.

EINE EXPERIMENTELLE UNTERSUCHUNG DER TURBULENTEN PRANDTL-ZAHL FÜR LUFT MIT EINBLASUNG UND ABSAUGUNG

Zusammenfassung—Aus dem mittleren Geschwindigkeits- und Temperaturprofildaten von Simpson [5] und Whitten [6] wurden experimentelle Werte für Pr_t bei turbulenten inkompressiblen Luftgrenzschichten ($Pr = 0{,}71$) mit Ausblasung, ohne Ausblasung und mit Absaugung erhalten. Für das bei der Gewinnung dieser Ergebnisse angewandte Verfahren wird eine Beschreibung gegeben. Im inneren Ähnlichkeitsgebiet ist $Pr_t > 1$, im äusseren ist $Pr_t < 1$. Diese Ergebnisse stehen in Übereinstimmung mit Ludweig's [2] Ergebnissen in Rohren und zeigen keinen Einfluss von Ausblasung oder Absaugung auf Pr_t. Das Jenkins-Modell [21], das ungleichem Verlust von Impuls und thermischer Energie eines Wirbels im Flug, für Medien mit $Pr = 1$ Rechnung tröigt, beschreibt die Variation von Pr_t im inneren Gebiet innerhalb der experimentellen Unsicherheit der Daten. Unter Benutzung von Hinze's [14] Vorschlag, dass die Wärmediffusion eine Kombination aus dem Transport durch einen Gradienten und durch grosse Wirbel ist, wird ein neues Modell entwickelt, das die Bedingung $Pr_t < 1$ im äusseren Gebiet berücksichtigt. Auf diesen Modellen basierende Berechnungen liegen innerhalb der Streugrenzen der experimentellen Ergebnisse und deuten keinen Einfluss von Ausblasung oder Absaugung auf Pr_t an.

ЭКСПЕРИМЕНТАЛЬНОЕ ИССЛЕДОВАНИЕ ТУРБУЛЕНТНОГО ЧИСЛА ПРАНДТЛЯ ДЛЯ ВОЗДУХА ПРИ ВДУВЕ И ОТСОСЕ

Аннотация—Из данных Симпсона [5] и Уиттена [6] для профилей средней скорости и температуры получены экспериментальные значения для Pr_t в турбулентных пограничных слоях несжимаемой жидкости ($Pr = 0{,}71$) со вдувом, без вдува и с отсосом. Описана методика получения этих результатов. Во внутренней обпасти подобия в ядре $Pr > 1$, а во внешней $Pr_t < 1$. Эти результаты согласуются с данными Людвига [2] для трубы и показывают, что вдув и отсос не влияют на Pr_t. Найдено, что моделб дженкинса [21], учитывающая неодинаковую потерю количества движения и тепловой энергии вихря для жидкостей с $Pr = 1$, описывает изменение Pr_t во внутренне области в пределах точности эксперимента. Используя предложение Хинца [14], что диффузия

тепла может быть комбинацией переноса градиента и большого вихря, разработана новая модель для $Pr_t < 1$ во внешней области. Расчеты, основанные на этих моделях, лежат в прелелах точности экспериментальных результатов и показывают, что вдув и отсос не оказывают влияния на Pr_t.